Original Article

JOURNAL OF REINFORCED PLASTICS & COMPOSITES

Journal of Reinforced Plastics and Composites
0(0) 1–9
© The Author(s) 2015
Reprints and permissions:
sagepub.co.uk/journalsPermissions.nav
DOI: 10.1177/0731684415573813
jrp.sagepub.com
SAGE

Damage monitoring of polymer-lined carbon fibre-reinforced plastic using small-diameter fibre Bragg grating sensors

Shin-ichi Takeda[1], Tomohiro Yokozeki[2] and Toshio Ogasawara[1]

Abstract

Small-diameter fibre Bragg grating sensors were embedded in liquid crystalline polymer-lined carbon fibre-reinforced plastics to detect internal microscopic damages that are barely visible in operation. The coupon specimen caused matrix cracks and liner debonding under tensile loading, which represented distinctive damages in a composite overwrapped pressure vessel. The reflection spectra from the fibre Bragg grating sensors were measured in the loading–unloading tests. As the number of matrix cracks increased, the width of the spectrum gradually increased. The change in the measured results were validated by spectra simulated using the axial strain distribution in the fibre Bragg grating sensor. Moreover, the influence of damage morphology on the reflection spectrum was investigated on the basis of the analytical results for both embedded and surface-bonded fibre Bragg grating sensors. The embedded fibre Bragg grating sensor was less sensitive than the surface-bonded fibre Bragg grating sensor for distinguishing among the damage modes, such as matrix cracks, liner debonding and liner failure. The effectiveness of strain-based monitoring using fibre Bragg grating sensor was demonstrated for evaluation of the microscopic damages in polymer-lined carbon fibre-reinforced plastics.

Keywords

Fibre Bragg grating sensors, carbon fibre-reinforced plastics, matrix cracks, damage monitoring

Introduction

Carbon fibre-reinforced plastic (CFRP) laminates are indispensable materials for use in liquid propellant tanks, which is accounted for most of the structural weight in space transportation systems. Liquid nitrogen (−253.5°C boiling point) and liquid oxygen (−183°C boiling point) are often used as propellants. The applications of CFRP cryogenic tanks have been studied for over the past two decades.[1–9] Although the required pressure is low compared with general purpose high-pressure vessels, a CFRP tank is exposed to cryogenic temperatures. Moreover, because the curing temperature of high-performance CFRP is approximately 180°C, a difference in the thermal expansions of carbon fibres and resins evolves non-negligible thermo-mechanical stresses, which were also influenced by the cure shrinkage and vitrification, and tool-part interaction. These stresses facilitate the onset and accumulation of matrix cracks. An important issue related to cryogenic CFRP tanks is the fuel gas leakage that occurs via microscopic damages, such as matrix cracks, fibre/matrix debonding and delamination.[10–16] This intractable problem has spurred the research and development of composite overwrapped pressure vessels (COPVs), such as a non-structural thin liner wrapped with CFRP.

Many studies report the use of an aluminium liner for COPVs, whereas other studies have involved the

[1]Institute of Aeronautical Technology, Japan Aerospace Exploration Agency, Japan
[2]Department of Aeronautics and Astronautics, The University of Tokyo, Japan

Corresponding author:
Shin-ichi Takeda, Institute of Aeronautical Technology, Japan Aerospace Exploration Agency, 6-13-1 Osawa, Mitaka-shi, Tokyo 181-0015, Japan.
Email: takeda.shinichi@jaxa.jp

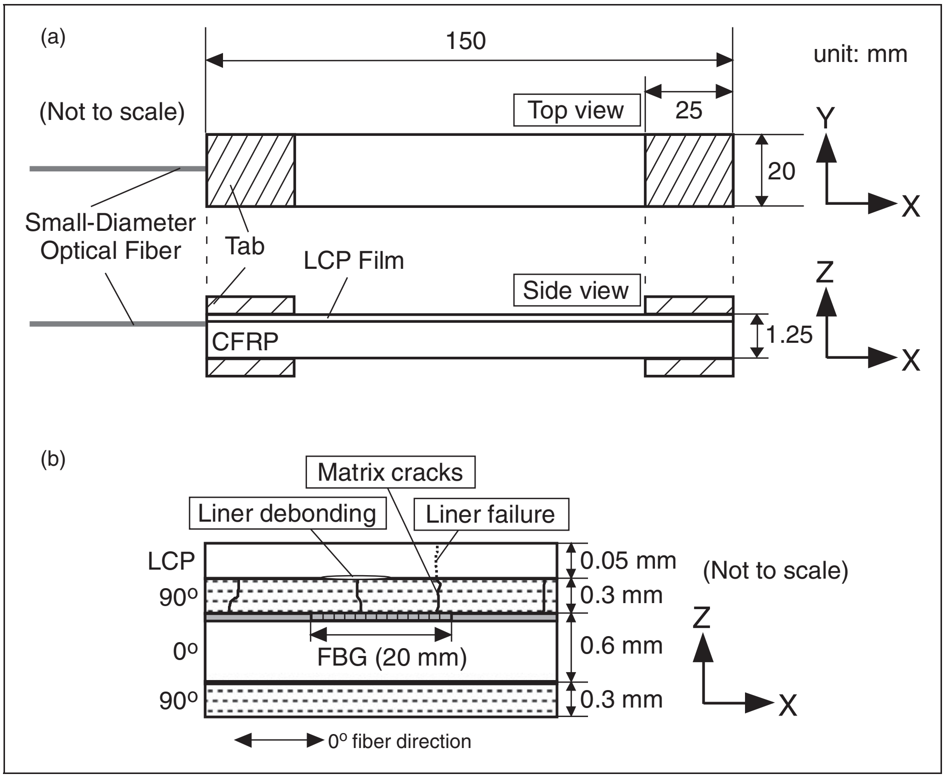

Figure 1. Schematic of the CFRP specimen lined with LCP film. (a) Overall dimensions and (b) Cross-sectional view around embedded FBG sensor.

application of polymer films to achieve lighter weight COPVs.[17–20] Our group has previously used various polymer films as liner materials in CFRPs to investigate the relationship between microscopic damages and the mechanical properties of the plastics.[21] The results indicated that although the appropriate combination of polymer films and CFRPs prevented liner failure under tensile loading, it caused matrix cracks and liner debondings. Such damages are difficult to avoid when a typical CFRP is selected as a structural material for use in COPVs. Consequently, the structural health-monitoring technology offers a practical solution to assure the structural integrity of the CFRP tank.

One of the most commonly used and broadly deployed optical sensors is the fibre Bragg grating (FBG), which has been frequently used for monitoring of COPVs.[22–24] The FBG sensors have been mainly used for acoustic emission (AE) monitoring and strain monitoring. AE monitoring has high sensitivity to progressive damage, whereas strain monitoring is straightforward because the results can be compared with those from a structural analysis of the COPV. We believe that the strain-based monitoring is desirable if it can reliably evaluate the damage accumulation in COPVs. The embedding of the FBG sensor in CFRP laminates has been demonstrated to be an effective approach for

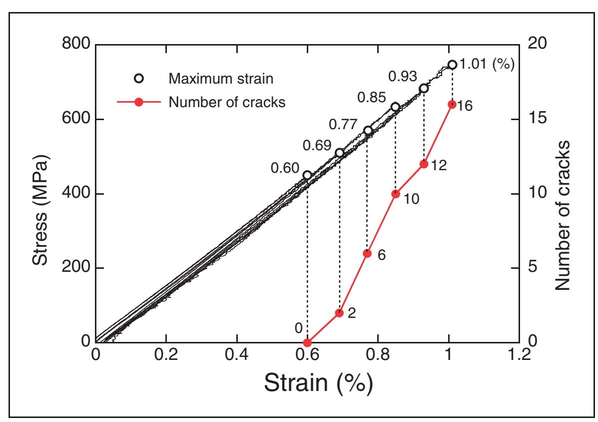

Figure 2. Relationship between maximum strain and number of cracks during load–unload tests.

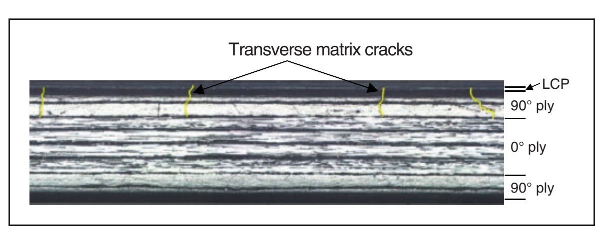

Figure 3. Optical micrograph of the edge of the specimen.

detecting microscopic damages, such as matrix cracks and delaminations.[25–27] Thus, in this study, we focused on monitoring of microscopic damages in inner surface lined CFRP tanks using a small-diameter FBG sensor that was developed to be embedded without adversely affecting the strength of the host material. The embedded FBG sensor was used in CFRP cross-ply laminates lined with liquid crystalline polymer (LCP) film; we also used this polymer lined composite in our previous study.[21]

Table 1. Mechanical properties of the carbon fibre-reinforced plastic (CFRP) and liquid crystalline polymer (LCP).[21]

		CFRP	LCP
Elastic moduli (GPa)	E_1	157	
	E_2	8.9	7.6
	G_{12}	4.8	
Poisson's ratios	ν_{12}	0.35	
	ν_{23}	0.45	0.3
Coefficients of thermal expansion ($\times 10^{-6}$ K^{-1})	α_{11}	−0.5	1
	α_{22}	22.5	

Experiment programme

Small-diameter FBG sensors

FBG sensors have a periodic variation in the refractive index along a certain length of a single-mode optical fibre. When a broadband light is launched into the FBG sensor, it reflects a narrowband light. The centre wavelength of the reflected light, λ, is given as follows

$$\lambda = 2n \times \Lambda \tag{1}$$

where n and Λ are the average refractive index and the grating period, respectively. When an axial strain, ε_1, and two transverse strains, ε_2 and ε_3, are applied to the FBG sensor, the n and Λ are expressed as follows

$$n = n_0 - \frac{n_0^3}{2}\left[P_{12}\varepsilon_1 + (P_{11} + P_{12})\frac{\varepsilon_2 + \varepsilon_3}{2}\right] \tag{2}$$

$$\Lambda = (1 + \varepsilon_1)\Lambda_0 \tag{3}$$

In these equations, n_0 and Λ_0 are the initial average refractive index and the initial grating period at a

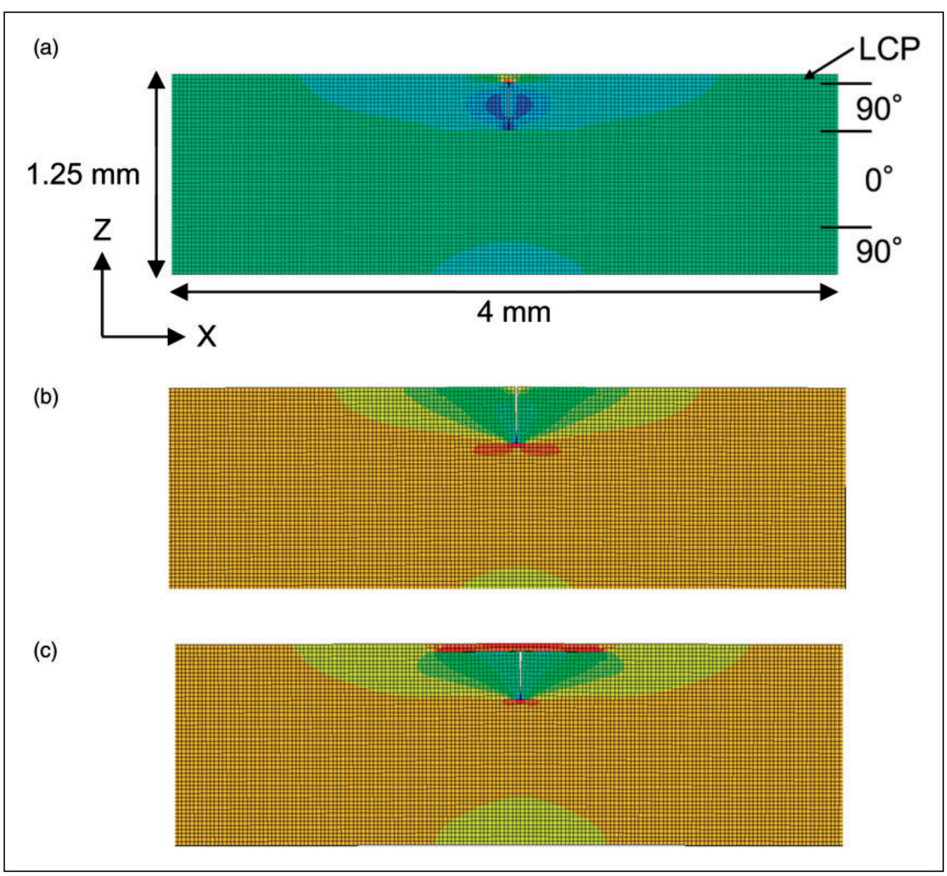

Figure 4. Contour plots of the strain along the carbon fibre direction of the 0° ply. (a) A single transverse crack (b) A single crack with liner failure and (c) A single transverse crack with liner debonding of 1 mm.

strain-free state, respectively, and P_{11} and P_{12} are Pockel constants. When a uniform strain is applied to the FBG sensor, the reflection spectrum shifts while maintaining its original narrow shape because n and Λ are also uniform along the entire length of the sensor. However, the spectrum is highly sensitive to non-uniform strains.[28] The form of reflection spectrum will change depending on non-uniform strains induced by damages in composites.[29–31]

Small-diameter FBG sensors (Hitachi Cable, Ltd.) have been reported to prevent strength deterioration when embedded in CFRP laminates.[32] Thus, in this study, we used the embedded small-diameter FBG sensor to detect microscopic damages in polymer-lined CFRP laminates. The small-diameter FBG sensors were fabricated in small-diameter optical fibres coated with polyimide. The core and cladding diameters were 6.5 µm and 40 µm, respectively. The outer diameter of the polyimide coating was 52 µm. The length of the grating was 20 mm, and the grating period was approximately 0.5 µm. The profile of the refractive index modulation was controlled as a cosine function to suppress the side lobe of the reflection spectrum. The monitoring system was composed of a circulator, an ASE light source (ASE-FL7002, Thorlabs, Inc.) and a spectrum analyser (MN9674A, Anritsu Corporation).

Table 2. Optical properties of the small-diameter fibre Bragg grating (FBG) sensor.[26]

Pockel constants	P_{11}	0.113
	P_{12}	0.252
Initial average refractive index	n_0	1.454
Initial grating period (nm)	Λ_0	535.84
Index modulation	Λ_n	5.2×10^{-4}
Refractive index of cladding	n_{cl}	1.444

Specimens and load–unload tests

The materials were a unidirectional CFRP prepreg (IM600/#133, Toho Tenax Co., Ltd.) and an LCP film with a thickness of 50 µm (Vecstar-FA50, KURARAY CO., LTD.). The prepregs with one LCP film were co-cured at 180°C for 2 h in an autoclave. The stacking

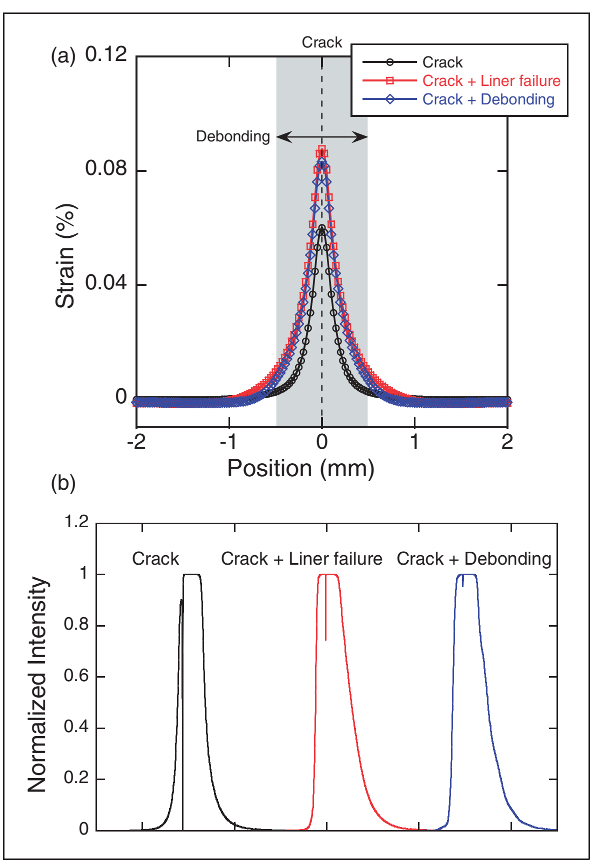

Figure 5. Influence of the damage morphology for the embedded FBG sensor. (a) Strain distribution in the FBG sensor and (b) Reflection spectra.

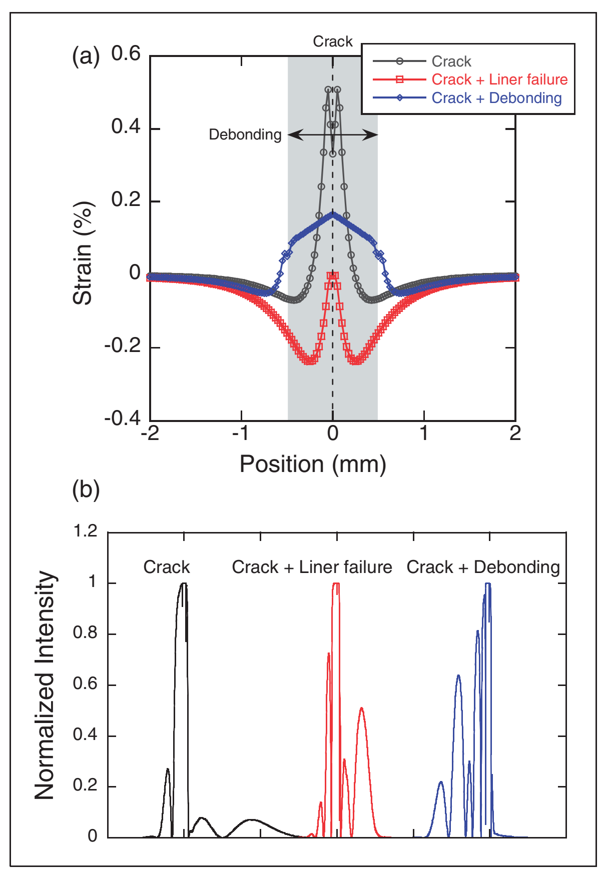

Figure 6. Influence of the damage morphology for the surface-bonded FBG sensor. (a) Strain distribution in the FBG sensor and (b) Reflection spectra.

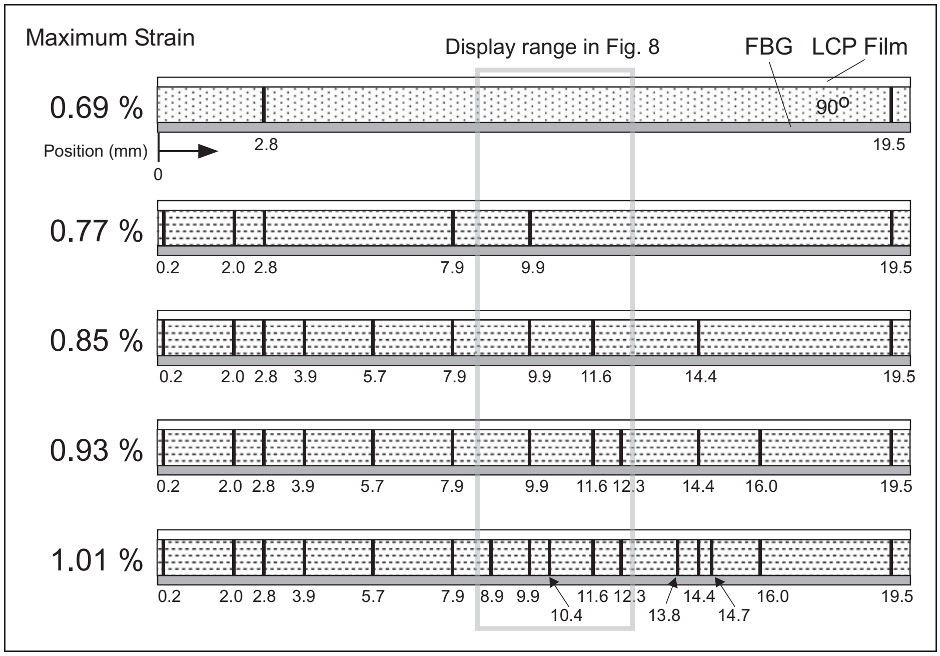

Figure 7. Schematic of the crack growth in the upper 90° ply in the specimen. The numbers indicate the distance of the crack from the left-side edge in the FBG sensor.

sequence was [LCP/$90_2/0_4/90_2$], which was sufficient for the purpose of this study, although the prepreg/film laminate was not entirely symmetric about the thickness direction. The dimensions and cross-sectional view of a test specimen are shown in Figure 1. The optical fibres were embedded into the 0° ply in contact with the 0°/90° interface in the specimen. The FBG of 20 mm gauge length was placed at the centre of the specimen.

The load–unload tests were performed under displacement control at a rate of 0.25 mm/min. The strain was evaluated using an extensometer with a gauge length of 25 mm and a travel distance of −2.5 to 5 mm (634.12, MTS Systems Corporation). The test was stopped at a pre-determined load level, and the test specimen was subsequently unloaded and released from the testing machine. The reflection spectra of the FBG were measured using a spectrum analyser. Transverse cracks of the 90° ply were observed from the edge of the specimen using an optical microscope because in our previous study, using the same specimen configuration, we observed that cracks penetrated through the overall width of the specimen.[21] The range of the observation corresponded to the embedding location of the FBG. After the observation, the test was repeated several times until the final failure of the specimen.

Results and discussion

Experimental results

The relationship between the maximum strain and the number of cracks during the load–unload tests are shown in Figure 2. With an increase in the applied strain and the number of cracks, the stiffness of the specimen decreased gradually. Figure 3 shows microscopic damages in the specimen by optical microscopy. The transverse cracks were only observed in the upper 90° ply because the bonded LCP film involved larger thermal residual tensile stress in the ply than that in the lower 90° ply. This result indicates that the coefficient of thermal expansion (CTE) of the LCP film would be smaller than that of the 90° ply in the CFRP, given that their stiffnesses are similar. The liner debonding was approximately 1 mm for almost all the crack tips, as observed from the appearance of the specimen.

Influence of damage morphology on the reflection spectrum from FBG sensors

Before verifying the experimental results, we investigated the influence of damage morphology on the reflection spectrum by simulating the spectrum. Finite element analysis was performed using the commercial software ABAQUS to obtain the axial strain distribution in the FBG sensor. The FBG sensor was omitted in the model because the strain in the CFRP has been previously demonstrated to be similar to the axial strain in the embedded FBG sensor.[33] The entire specimen was modelled using 2D solid elements under plane strain conditions. The analyses were for a single transverse crack, a single transverse crack with liner failure and a single transverse crack with liner debonding of 1 mm. All the damage types were represented by

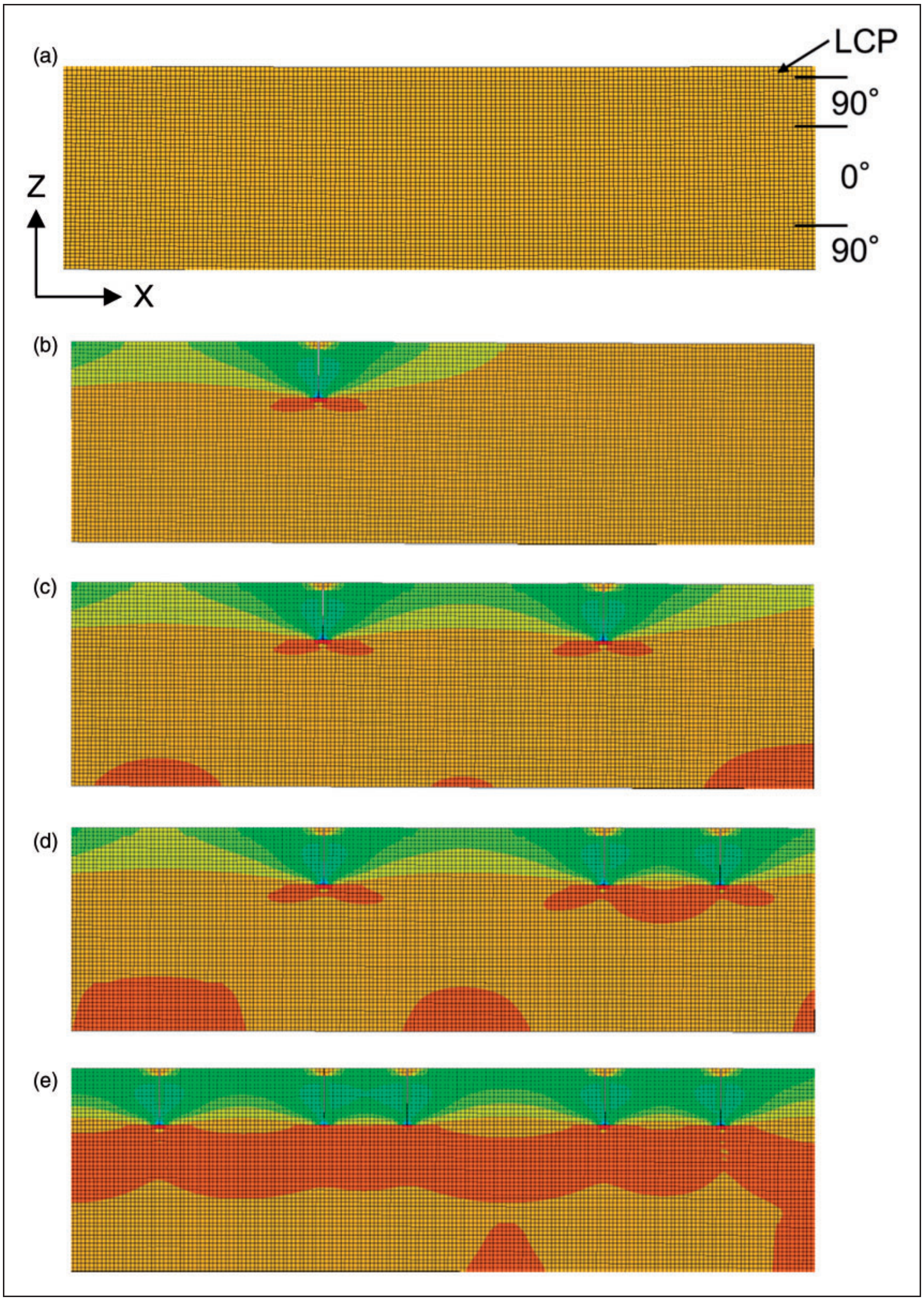

Figure 8. Contour plots of the strain along the carbon fibre direction of the 0° ply. The display range corresponds to the square-shaped area in Figure 7. (a) 0.69%, (b) 0.77%, (c) 0.85% (d) 0.93% and (e) (e) 1.01%.

duplicate nodes in each model. The material properties used in the analysis are summarized in Table 1. The CTE of the LCP was assumed to be $1 \times 10^{-6}\,K^{-1}$ because it is smaller than that of the 90° ply in the CFRP and is typically a positive value for polymers. A temperature change from 180°C (cure temperature) to 25°C (room temperature) was used in the model.

Figure 4 shows a contour plot of the strain along the carbon fibre direction of the 0° ply. The strain concentration area changed depending on the damage morphology. An axial strain distribution in the FBG sensor was obtained by the strain outputs of the elements at the same location as the sensor. The reflection spectra were simulated by commercial software "IFO Gratings" (Optiwave Corporation) which solves couple mode equations with transfer matrix method. The properties of the FBG sensor used in the simulation of the spectrum are summarized in Table 2.

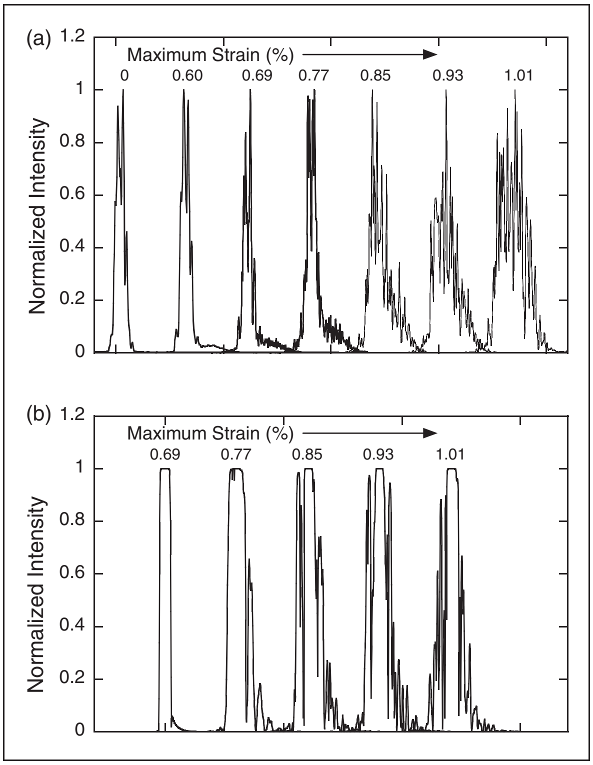

Figure 9. Changes in the reflection spectra during load–unload tests. (a) Measured spectra and (b) Calculated spectra.

The influence of the damage morphology on the axial strain distributions and corresponding spectra are shown in Figure 5. There is no x-axis in the graph of the reflection spectra because the three spectra were included in one graph by shifting the wavelength of the spectrum. The intensity of the reflection spectrum was normalized by the intensity of the highest component. The transverse crack changed the shape of the spectrum from a simple single peak to a split single peak. However, in the case of liner failure or debonding, the shape of the spectrum deformed only slightly because the shape of the strain distribution was very similar for all analyses. This result indicates that the embedded FBG sensor can detect the transverse crack but has difficulty in distinguishing each damage mode.

If the FBG sensor was attached to the surface of the LCP film, where the strain changed substantially because of the damages, the damage modes would likely be distinguishable. The influence of the damage morphology on the analytical results for the surface-bonded FBG sensor was investigated, as shown in Figure 6. The different shape of the strain distribution for the analysis directly reflected the change in the shape of the spectrum. This monitoring method using a surface-bonded FBG sensor is effective in damage classification; however, to enable its practical use, introducing the FBG sensor to the inner surface of the liner and ensuring the reliability of the adhesive bond are critical problems that must be overcome.

Verification of measured results by simulated reflection spectra

The observed crack locations in the range of the embedded FBG are summarized in Figure 7. As the maximum strain was increased, a new crack emerged between the cracks. The number of cracks shown in this figure corresponds to that shown in Figure 2. The strain distribution was calculated by finite element analysis using the crack location results. Although liner debonding increased at almost all the crack tips, we ignored it in the analysis because of its small influence on the shape in the spectrum. Figure 8 shows the strain distributions around the central part of the FBG. The location of strain concentration in the FBG sensor corresponded to the location of cracks in the upper 90° ply. The spectra were simulated on the basis of the strain distributions and the results were compared with the measured spectra, as shown in Figure 9. The shape in the calculated spectra at 0% and 0.60% maximum strain should be purely one peak because there are no matrix cracks in the analysis. Nevertheless, the corresponding measured spectra were distorted by the non-uniform strain distribution due to a slight misalignment of the embedded FBG sensor. As the maximum strain and the number of cracks increased, the widths of both the measured and calculated spectra increased. These changes could be used to indicate an increase in the number of matrix cracks in inner surface lined CFRP tanks.

Conclusions

Strain-based monitoring using an embedded small-diameter FBG sensor was applied to LCP-lined CFRP laminates at an ambient temperature. The larger mismatch of CTEs causes the larger thermomechanical stresses between the plies at a cryogenic environment, which would trigger matrix cracks at an earlier stage. The monitoring technique is able to use screening process or detection of barely visible fatigue cracks in COPVs. An increase in the width of the spectrum from the FBG sensor indicated an increase in matrix cracks; this correlation was validated by the calculated results. The influence of the location of the FBG on the reflection spectrum was investigated analytically. The surface-bonded FBG sensor indicated the potential to distinguish among damage modes, such as matrix cracks, matrix cracks with liner failure, and matrix cracks with liner debonding. However, the embedded FBG sensor was used without ensuring the reliability of the adhesive bond, which would be required for its practical use. The installation position of the FBG sensor should be decided by the pre-analysis of whether the spectral change due to envisioned damage modes can be detected under the usage environment.

Conflict of interest

None declared.

Funding

This research received no specific grant from any funding agency in the public, commercial, or not-for-profit sectors.

References

1. Macconochie IO, Davis RB and Lemessurier RW. Structural design of integral tankage for advanced space transportation systems. *23rd Structures, Structural Dynamics and Materials Conference*, AIAA: 82-0634, 1982.
2. Knoll RH, England JE and Macneil PN. Development and Test of the shuttle/centaur cryogenic tankage thermal protection system. *22nd Thermophysics Conference*, AIAA-87-1557, 1987.
3. Robinson MJ. Composite cryogenic propellant tank development. *35th Structures, Structural Dynamics, and Materials Conference*, AIAA-94-1375-CP, 1994.
4. Arritt BJ, Wegner PM, Fosness ER, et al. Composite tank development efforts at the Air Force Research Laboratory Space Vehicles Directorate. *AIAA Space 2001 Conference and Exposition*, AIAA-2001-4606, 2001.
5. Morino Y, Shimoda T, Morimoto T, et al. Applicability of CFRP materials to the cryogenic propellant tank for reusable launch vehicle (RLV). *Adv Compos Mater* 2001; 10: 339–347.
6. Aoki T, Ishikawa T, Kumazawa H, et al. Cryogenic mechanical properties of CF/polymer composites for tanks of reusable rockets. *Adv Compos Mater* 2001; 10: 349–356.
7. Messinger R and Pulley J. Thermal–mechanical cyclic test of a composite cryogenic tank for reusable launch vehicles. *44th AIAA/ASME/ASCE/AHS/ASC Structures, Structural Dynamics, and Materials Conference*, AIAA 2003-1766, 2003.
8. Achary DC, Biggs RW, Bouvier CG, et al. Composite development & applications for cryogenic tankage. *46th AIAA/ASME/ASCE/AHS/ASC Structures, Structural Dynamics, and Materials Conference*, AIAA 2005-2160, 2005.
9. Johnson TF, Sleight DW and Martin RA. Structures and design phase I summary for the NASA composite cryotank technology demonstration project. *54th AIAA/ASME/ASCE/AHS/ASC Structures, Structural Dynamics, and Materials Conference*, AIAA 2013-1825, 2013.
10. Kumazawa H, Aoki T and Susuki I. Analysis and experiment of gas leakage through composite laminates for propellant tanks. *AIAA J* 2003; 41: 2037–2044.
11. Roy S and Benjamin M. Modeling of permeation and damage in graphite/epoxy laminates for cryogenic fuel storage. *Compos Sci Technol* 2004; 64: 2051–2065.
12. Yokozeki T and Ogasawara T. Evaluation of gas leakage through composite laminates with multilayer matrix cracks: cracking angle effects. *Compos Sci Technol* 2006; 66: 2815–2824.
13. Bechel V, Negilski M and James J. Limiting the permeability of composites for cryogenic application. *Compos Sci Technol* 2006; 66: 2284–2295.
14. Yokozeki T, Aoki T and Ishikawa T. Experimental cryogenic gas leakage through damaged composite laminates for propellant tank application. *J Spacecraft Rockets* 2005; 42: 363–366.
15. Yokozeki T, Ogasawara T, Aoki T, et al. Experimental evaluation of gas permeability through damaged composite laminates for cryogenic tank. *Compos Sci Technol* 2009; 69: 1334–1340.
16. Yokozeki T, Kuroda A, Yoshimura A, et al. Permeation-after-impact properties of CFRP laminates for use on propellant tank. *T Jpn Soc Aeronaut Space Sci Space Technol Jpn* 2009; 7: 19–23.
17. Guiles M. Liquid crystal polymer cryogenic storage tank with reduced thermal loss and weight. *31st Joint Propulsion Conference and Exhibit*, AIAA 95-2355, 1995.
18. Ishikawa T, Aoki T and Morino Y. Perspective in research activities cryogenic composite tanks for RLV in Japan. *AIAA Space 2001 Conference and Exposition*, AIAA 2001-4605, 2001.
19. Kooij T, Oscar J and Beukers A. A full composite LOX fuel tank for a hybrid rocket. In: *Proceedings of the European Conference Spacecraft Structures*. ESASP-468 2001; pp.187–192.
20. Sippel M, Kopp A, Mattsson D, et al. Advanced cryo-tanks research in CHATT. In: *Proceedings of the 5th European conference for aeronautics and space science*, Munich, Germany: EUCASS, 2013.
21. Yokozeki T, Yamagata T and Ogasawara T. Research on damage behaviors of CFRP laminates with polymer films for cryogenic tank application. *J Jpn Soc Compos Mater* 2008; 34: 3–13. (In Japanese).
22. Kang HK, Park JS, Kang DH, et al. Strain monitoring of a filament wound composite tank using fiber Bragg grating sensors. *Smart Mater Struct* 2002; 11: 848–853.
23. Graue R and Reutlinger A. Structural condition monitoring system for RLV tanks. In: *Proceedings of the 55th international astronautical congress*. IAC-04-V.5.07; 2004.
24. Mizutani T, Takeda N and Takaya H. On-board strain measurement of a cryogenic composite tank mounted on a reusable rocket using FBG sensors. *Struct Health Monitor* 2006; 5: 205–214.
25. Okabe Y, Yashiro S, Kosaka T, et al. Detection of transverse cracks in CFRP composites using embedded fiber Bragg grating sensors. *Smart Mater Struct* 2000; 9: 832–838.
26. Takeda S, Okabe Y and Takeda N. Delamination detection in CFRP laminates with embedded small-diameter fiber Bragg grating sensors. *Compos Part A* 2002; 33: 971–80.

27. Takeda S, Minakuchi S, Okabe Y, et al. Delamination monitoring of laminated composites subjected low-velocity impact using small-diameter FBG sensors. *Compos Part A* 2005; 36: 903–908.
28. Huang S, Ohn MM, Leblanc M, et al. Continuous arbitrary strain profile measurements with fiber Bragg gratings. *Smart Mater Struct* 1998; 7: 248–256.
29. Arjyal BP, Galiotis C, Ogin SL, et al. Residual strain and Young's modulus determination in cross-ply composites using an embedded aramid fibre strain sensor. *Compos Part A* 1998; 29: 1363–1369.
30. Mizutani T, Okabe Y and Takeda N. Quantitative evaluation of transverse cracks in carbon fiber reinforced plastic quasi-isotropic laminates with embedded small-diameter fiber Bragg grating sensors. *Smart Mater Struct* 2003; 12: 898–903.
31. Wang H, Ogin SL, Thorne AM, et al. Interaction between optical fibre sensors and matrix cracks in cross-ply GFRP laminates. *Part 2: Crack detection*. Compos Sci Technol 2006; 66: 2367–2378.
32. Takeda S, Okabe Y, Yamamoto T, et al. Detection of edge delamination in CFRP laminates under cyclic loading using small-diameter FBG sensors. *Compos Sci Technol* 2003; 63: 1885–1994.
33. Takeda S, Tsukada T, Sugimoto S, et al. Monitoring of water absorption in CFRP laminates using embedded fiber Bragg grating sensors. *Compos Part A* 2014; 61: 163–171.